

Study of a high spatial resolution ^{10}B -based thermal neutron detector for application in neutron reflectometry: the Multi-Blade prototype

F. Piscitelli^{a,b,*}, J.C. Buffet^a, J.F. Clergeau^a, S. Cuccaro^a, B. Guérard^a, A. Khaplanov^{a,c}, Q. La Manna^a, J.M. Rigal^a and P. Van Esch^a

^a *Institut Laue-Langevin (ILL),
6, Jules Horowitz, 38042 Grenoble, France.*

^b *Department of Physics, University of Perugia,
Piazza Università 1, 06123 Perugia, Italy.*

^c *European Spallation Source,
P.O. Box 176, SE-22100 Lund, Sweden.*

E-mail: piscitelli@ill.fr

ABSTRACT: Although for large area detectors it is crucial to find an alternative to detect thermal neutrons because of the ^3He shortage, this is not the case for small area detectors. Neutron scattering science is still growing its instruments' power and the neutron flux a detector must tolerate is increasing. For small area detectors the main effort is to expand the detectors' performances.

At Institut Laue-Langevin (ILL) we developed the Multi-Blade detector which wants to increase the spatial resolution of ^3He -based detectors for high flux applications. We developed a high spatial resolution prototype suitable for neutron reflectometry instruments. It exploits solid ^{10}B -films employed in a proportional gas chamber. Two prototypes have been constructed at ILL and the results obtained on our monochromatic test beam line are presented here.

KEYWORDS: thermal neutron detectors; Boron-10; solid neutron converters; neutron reflectometry.

*Corresponding author.

Contents

| | |
|-----------------------------------|-----------|
| 1. Introduction | 1 |
| 2. The Multi-Blade concept | 3 |
| 3. Multi-Blade version V1 | 6 |
| 3.1 Mechanical study | 6 |
| 3.2 Mechanics | 7 |
| 3.3 Results | 11 |
| 3.3.1 Operational voltage | 11 |
| 3.3.2 Gain | 12 |
| 3.3.3 Efficiency | 13 |
| 3.3.4 Uniformity | 13 |
| 3.3.5 Spatial resolution | 14 |
| 4. Multi-Blade version V2 | 15 |
| 4.1 Mechanical study | 15 |
| 4.2 Mechanics | 17 |
| 4.3 Results | 19 |
| 4.3.1 Operational voltage | 19 |
| 4.3.2 Efficiency | 19 |
| 4.3.3 Uniformity | 21 |
| 4.3.4 Spatial resolution | 21 |
| 4.3.5 Dead time | 23 |
| 5. Conclusions | 25 |

1. Introduction

Although the ^3He shortage pushes the research of alternatives for large area detectors, this is not the case for small area detectors, where the main effort is to expand the detectors' performances. At Institut Laue-Langevin (ILL) in Grenoble (France) we developed the Multi-Blade detector which wants to push the limit of spatial resolution of ^3He -based detectors for high flux applications. The Multi-Blade was conceived to be a detector suitable for neutron reflectometry instruments which require a high spatial resolution.

Moreover, neutron scattering science is still growing its instruments' power and the neutron flux a detector must tolerate is increasing. The peak brightness at the new European Spallation Source (ESS) in Lund (Sweden) will be higher than that of any of the short pulse sources, and will be

more than one order of magnitude higher than that of the world's leading continuous source. The time-integrated brightness at ESS will also be one to two orders of magnitude larger than is the case at today's leading pulsed sources [1], [2]. The Multi-Blade can also address the counting rate capability of ^3He detectors looking forward higher fluxes.

A neutron detector for a reflectometer is in general compact in size (about $400 \times 250\text{mm}^2$ [3]) and it is characterized by a non-uniform spatial resolution. In order to achieve the needed angular resolution a high spatial resolution is only needed in one direction and it is of the order of 1mm [4]. Such a resolution is really needed only for off-specular studies. To be more precise a Position Sensitive Detector (PSD) is necessary when not only specular reflection occurs but one wants to quantify more sample features, e.g. off-specular reflection arising from the presence of in-plane structures.

For a large number of applications only the specular reflection is needed and the other detector coordinate is generally integrated over. The 1mm spatial resolution is still feasible with ^3He detector but in many areas of soft and hard matter research science, the amount of material to investigate is rather limited. Partly because the fabrication of larger samples is too expensive or not feasible, yet, partly because the interesting features depend on the size. The development of a neutron reflectometer optimized for small samples is under study [5]. There is a great deal of interest in expanding the technique of neutron reflectometry beyond static structural measurements of layered structures to kinetic studies [6]. The time resolution for kinetic studies is limited by the available neutron flux.

For a reflectometer the actual neutron flux reaching the sample is a small fraction of the incoming neutron beam. In [6] and [7] a new instrument layout is presented to open the possibility of sub-second kinetic studies, however this requires very high spatial resolution detectors. The wanted resolution, well beyond the reasonable limit of the ^3He technology, is $\Delta x = 0.2\text{mm}$; required in one dimension only (the other dimension can be summed) [6].

CCD cameras instead of gaseous detectors can be used to improve the spatial resolution but Time-of-Flight measurements are not possible.

Moreover, ^3He -based detectors are also limited in counting rate capability by the space charge effect.

The Multi-Blade detector represents a promising alternative to ^3He -based detectors, to accomplish the high spatial resolution and the high count rate capability needed in the new applications of neutron reflectometry. This alternative exploits solid ^{10}B -films employed in a proportional gas chamber. The challenge with this technique is to attain a suitable detection efficiency which is about 63% for the Figaro [3] detector at 2.5\AA . A suitable detection efficiency can be achieved by operating the ^{10}B conversion layer at grazing angle relative to the incoming neutron direction. The Multi-Blade design is based on this operational principle and it is conceived to be modular in order to be adaptable to different applications. Two prototypes have been developed at ILL and the results obtained on our monochromatic test beam line are presented here. A significant concern in a modular design is the uniformity of detector response. Several effects might contribute to degrade the uniformity and they have to be taken into account in the detector concept: overlap between different substrates, coating uniformity, substrate flatness, etc.

2. The Multi-Blade concept

The Multi-Blade concept was already introduced at ILL in 2005 [8] and a first prototype was realized in 2012 [9]. Its design is conceived to be modular in order to be versatile to be applied in many applications on several instruments. The Multi-Blade exploits solid ^{10}B -films employed as a neutron converter in a proportional gas chamber as in [10]. The challenge with this technique is to attain a suitable detection efficiency. This latter can be achieved by operating the ^{10}B conversion layer at grazing angle relative to the incoming neutrons direction. Moreover the inclined geometry leads to a gain in spatial resolution and as well in counting rate capability compared to ^3He detectors.

Figure 1 shows the Multi-Blade detector schematic, it is made up of several identical units called *cassettes*. Each *cassette* acts as an independent Multi Wire Proportional Chamber (MWPC) which holds both the neutron converter and the read-out system. The fully assembled detector is composed of several cassettes inclined toward the sample position. The angle subtended by each cassette looking at the sample position is kept constant in order to maintain the spatial resolution and the efficiency as uniform as possible.

The cassettes must be arranged taking into account an overlap between them in order to avoid dead space over the whole detector surface. If the instrument geometry changes the cassette arrangement in the detector should also change.

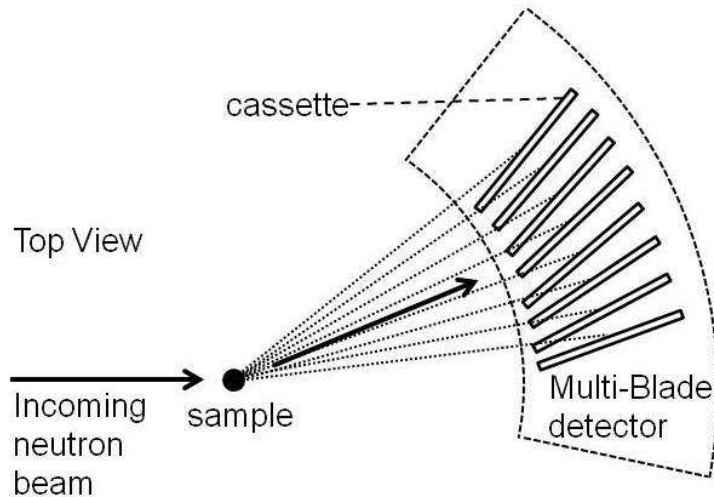


Figure 1. The Multi-Blade detector sketch (top view).

Each cassette should contain one or more neutron converters, e.g. $^{10}\text{B}_4\text{C}$ layers, and the read-out system that has to assure the two-dimensional identification of the neutron event. Figure 2 shows the cross-section of the cassette concept for three different configurations.

In the A and B solutions, in each cassette a single converter layer is facing each read-out system. The read-out is a wire plane and a strip plane placed orthogonally. The space between the strips and the converter is filled with stopping gas at atmospheric pressure to ensure the gas multiplication. The converter layer is polarized as well and acts as a cathode together with the strip plane; the wire

plane, on the other hand, acts as an anode plane.

In the C configuration a single wire plane performs the two-dimensional read-out through charge division on resistive wires. A single read-out system is facing two converter layers. The space between the two converters is filled with stopping gas. The two converter layers act as cathodes.

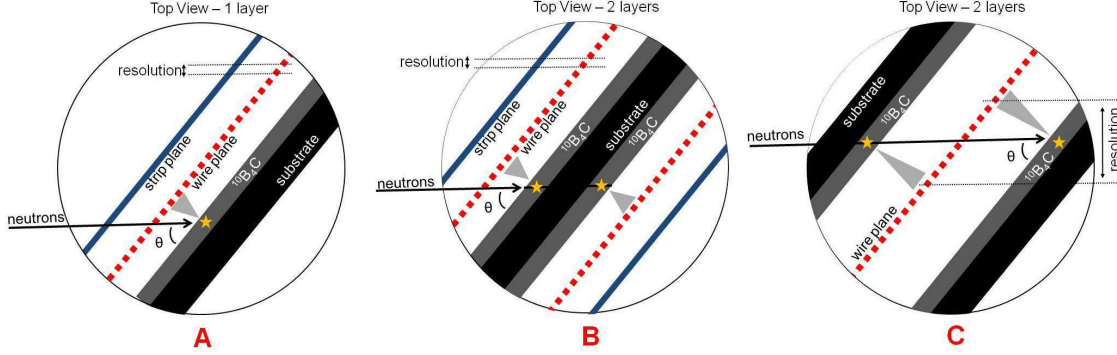


Figure 2. Cross-section of one cassette. Three options are shown: A, a single converter layer; B and C, with two converters.

Referring to configurations A and B, the identification of the position of a neutron event is the coincidence of wire and strip hits. The spatial resolution given by the strips does not depend on the inclination of the cassette. The spatial resolution given by the wire plane improves as the angle with the incoming neutron direction decreases. Note that if the detector is able to distinguish two events hitting on two consecutive wires, the spatial resolution is given by the wire pitch. Thanks to the inclination of the wire plane with respect to the incoming beam, this pitch is diminished by a factor $\sin(\theta)$ with θ the layer inclination. Hence, the spatial resolution is improved by the same factor. E.g. at $\theta = 5^\circ$, the resolution is improved by a factor about 10 ($1/\sin(\theta = 5^\circ) \sim 10$).

Moreover, the actual neutron flux over the detector would be divided by the same factor increasing its counting rate capability; the same flux is shared by several wires.

While the spatial resolution is improved by inclination in both options A and B in Figure 2, all the advantage of working at grazing angle is lost in the C configuration. In [11] can be found the actual implementation of such a detector. In options A and B the charge generated by neutron capture fragments in the gas gives a signal on the facing wires and strips. In the solution C, for a given incoming neutron direction there will be two regions on the converters where neutrons are converted. The smaller the angle at which we operate the detector, the larger is the distance between those two regions. The uncertainty on the conversion point is then given by this distance which is much bigger than the wire pitch. On the other hand, option C has half the number of read-out channels as compared to A and B. However, for us, high spatial resolution is crucial.

We decided to concentrate on the implementation of the option A and B.

In [9] has been derived how the solid converter layer efficiency increases as a function of its inclination. We decided to operate the Multi-Blade at either $\theta = 10^\circ$ or $\theta = 5^\circ$ in order to have significant detection efficiency and keeping the mechanics simple.

Figure 3 shows the detection efficiency for $^{10}\text{B}_4\text{C}$ layers ($\rho = 2.24 \text{ g/cm}^3$) calculated according to [12] and [13]. An energy threshold of 100 KeV is applied. We considered two possible configurations: options A and B in Figure 2, with one converter or two. On the left we show the neutron

detection efficiency, at 2.5\AA , as a function of the converter layer thickness for the solutions A and B. While the efficiency shows a maximum for the two layer option, it is saturated over $3\mu\text{m}$ for the single layer. The single converter option can attain a maximum efficiency of 28% at 10° and 44% at 5° (2.5\AA) to be compared with the double-layer efficiency of 37% and 54% respectively. The addition of the second layer, at $\theta = 5^\circ$ leads to an increase of the efficiency of about 10% with respect to the solution A. The advantage of having only one converter is that the coating can be of any thickness above $3\mu\text{m}$ and the efficiency is not affected, while for the two layer option its thickness should be well calibrated. Moreover, in the two layer configuration the substrate choice is also crucial because it should be kept as thin as possible to avoid neutron scattering and this leads to possible mechanical issues. On the solution A, the substrate choice can be more flexible because it has not to be crossed by neutrons.

On the right in Figure 3 we show the efficiency as a function of the neutron wavelength for the the single layer of thickness $3\mu\text{m}$ (configuration A). The Figaro's detector efficiency [3] efficiency is also plotted, it is a ^3He -based detector made up of 6.9mm tubes filled at 8bars . In the plots shown the detector gas vessel Aluminium window is also taken into account as a neutron loss. For the Figaro's detector we used a 5mm thick window, and, since the Multi-Blade detector will be operated at atmospheric pressure, we used a 2mm window. ^3He -based detectors' efficiency can be increased by increasing the ^3He pressure in the vessel; on the other hand, for a solid converter based detector the gas acts only as a stopping means, hence its pressure can be kept at atmospheric values. Consequently the gas vessel construction has less constraints.

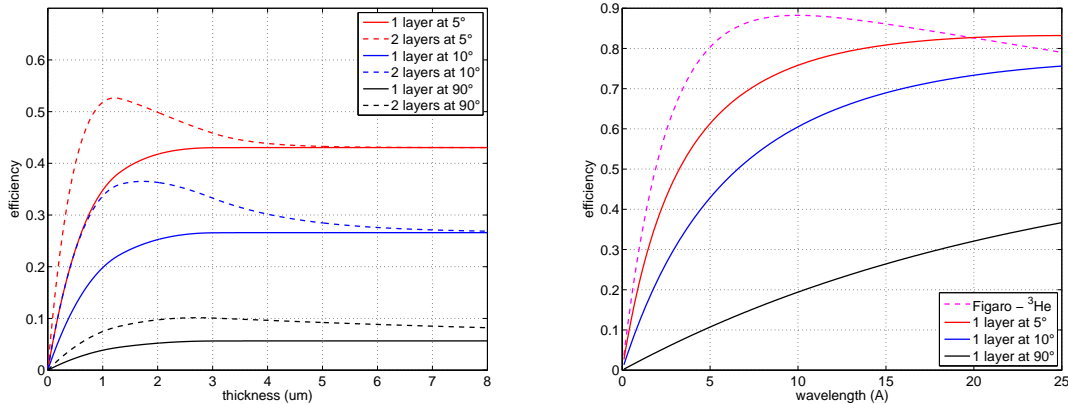


Figure 3. $^{10}\text{B}_4\text{C}$ layers ($\rho = 2.24\text{g/cm}^3$) detection efficiency at 2.5\AA as a function of the layer thickness for the options A and B for three inclinations (left), efficiency as a function of the neutron wavelength for three inclinations of a single $3\mu\text{m}$ layer (right). An energy threshold of 100KeV is applied. The efficiency of the Figaro's detector [3] is also shown (6.9mm tubes filled with 8bars of ^3He).

In each of the solutions proposed for the cassette concept, see Figure 2, the read-out system has to be crossed by neutrons before reaching the converter. The mechanical challenge in the read-out system construction is to minimize the amount of material on the neutron path to avoid scattering that can cause misaddressed events in the detector.

The cassettes must overlap to avoid dead spaces and the event loss, due to the zone where we switch the cassette, should be minimized. At the cassette edge electric field distortions and structure hold-

ing materials can cause a loss in the efficiency and consequently deteriorate the detector uniformity. In the prototype realization all these problems have been taken into account, two prototypes have been built in order to study the possible issues.

3. Multi-Blade version V1

3.1 Mechanical study

The prototype was conceived to clarify the advantages and disadvantages of the options A and B shown in Figure 2.

The detector works as a standard MWPC operated at atmospheric pressure stopping gas such as Ar/CO_2 (90/10).

Since we want to avoid neutrons to be scattered before reaching the converter layer, we need to minimize the amount of matter that has to be crossed by neutrons: the read-out system and the cassette window.

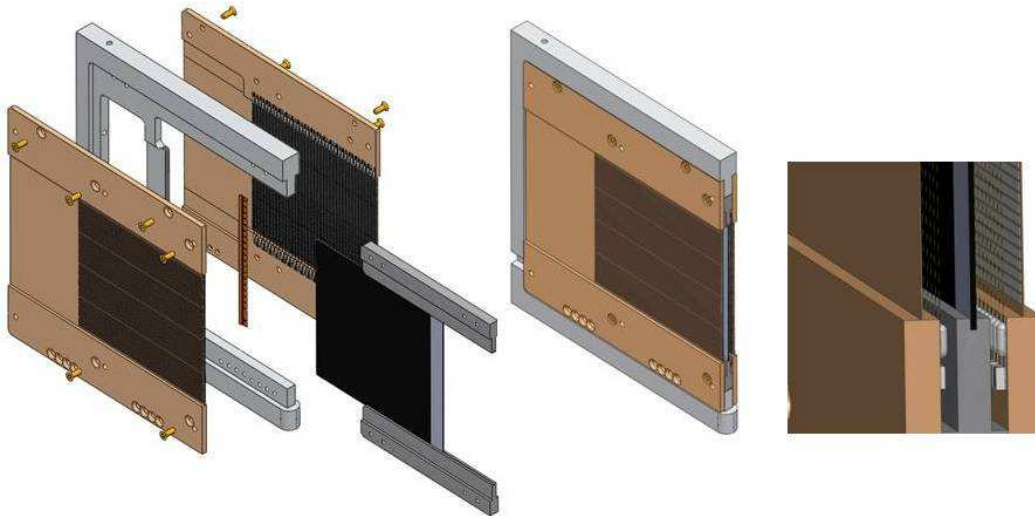


Figure 4. Exploded and assembled view of a cassette (left and center). Detail of a cassette (right): the two polyimide PCBs surrounding the coated blade.

Figure 4 shows a cassette drawing. An Aluminium substrate of thickness 0.5 mm is coated on both sides by a $^{10}B_4C$ -layer, i.e. a blade. One layer will work as a back-scattering layer and the second as a transmission layer [13]. The converter is surrounded symmetrically by two polyimide PCBs. Each of them holds a cathode strip plane and a anode wire plane. The converter layer substrate is grounded and it acts as a cathode plane. Therefore a half cassette is a complete MWPC containing one neutron converter layer and a two-dimensional read-out system.

The entire structure is supported by an Aluminium U-shaped holder. The latter shape was conceived to remove any material that can scatter the incoming neutrons. Moreover, each holder presents two gas inlets in order to supply the stopping gas directly inside the gap between the converter and the PCBs. The exhausted gas will flow out from the frontal opening of the cassette inside the gas vessel.

Figure 4 also shows the detail of an assembled cassette. The polyimide PCBs have to be crossed before neutrons can be converted, hence, in order to reduce the amount of material that can induce neutron scattering, and thus misaddressed detected events, those PCBs are as thin as possible according to the mechanical constraints in their inner active region. The strips are deposited on the polyimide and the anode wires are stretched orthogonally over the strip plane. The copper strips are 0.8mm wide and spaced by 0.2mm ; tungsten wires are $15\mu\text{m}$ thick and they are spaced by 2.5mm . The final electric signal is obtained by gas amplification on the anode wires placed in the gas volume. In order to decrease the number of read-out channels, anode wires and cathode strips are grouped by resistive chain for charge division read-out. Each full *cassette* has then 4 anode outputs and 4 cathodes outputs making 4 charge division read-out chains. The resistors are placed on the PCBs surface. This readout technique is cost-effective, but it is not the most performing concerning the count rate. If we want to take advantage of the high count rate capability a better readout technique must be used.

The polyimide PCBs are $60\mu\text{m}$ thick in the inner region: $25\mu\text{m}$ is the polyimide thickness and $35\mu\text{m}$ is the copper strips thickness.

The sensitive area of each cassette is $10 \times 9\text{cm}^2$ but, since it will be oriented at 10° with respect to the incoming neutron direction, the actual sensitive area offered to the sample is given by $(10\text{cm} \cdot \sin(10^\circ)) \times 9\text{cm} = 1.7 \times 9\text{cm}^2$. As a result, the actual wire pitch, at 10° , is improved down to 0.43mm .

The detector will be installed to have the better resolution in the direction of the reflectometry instrument collimation slits; i.e. the cassettes, which can be mounted either horizontally or vertically, will be oriented with the wires parallel to the instrument slits.

Figure 5 shows a drawing of 8 cassettes stacked one after the other and placed in the gas vessel.

As already mentioned, the main issue to be addressed in the final detector is the uniformity, as soon as it is made of several units, their arrangement is crucial to get a uniform response in efficiency. A misalignment in one of the modules can give rise to a drop in the efficiency or dead zones.

The cassettes have to be arranged in order to overlap to avoid dead zones. For this reason this detector is suitable for fixed geometry reflectometry instruments, where the distance between sample and detector is kept constant and the arrangement does not change.

The final prototype will be mounted in a gas vessel together with the gas distribution unit which splits the inlet in the several cassettes, and the electronic connections. This is illustrated in Figure 5.

Since the gas is flushed cost effective materials can be used because their outgassing is not an issue.

3.2 Mechanics

The first prototype (V1) consists of four cassettes operated at 10° . Given the cassette active region size, the prototype active area, considering their overlap is about $6 \times 9\text{cm}^2$.

Figure 6 shows a polyimide PCB. The latter is composed by a stack of three layers: two thick PCBs where in the middle is fixed a $25\mu\text{m}$ polyimide foil. The inner part is soft and the external part serves as a holder. 86 copper strips are deposited on the surface of the thin region (see Figure 7).

39 anode wires (37 active wires and 2 guard wires) are mounted and soldered on pads at 2mm distance from the cathode plane. Both for anodes and for cathodes a resistive chain is soldered on the rigid PCB. The total resistance is $6\text{K}\Omega$ for the anode chain and $8\text{K}\Omega$ for the cathode chain. At

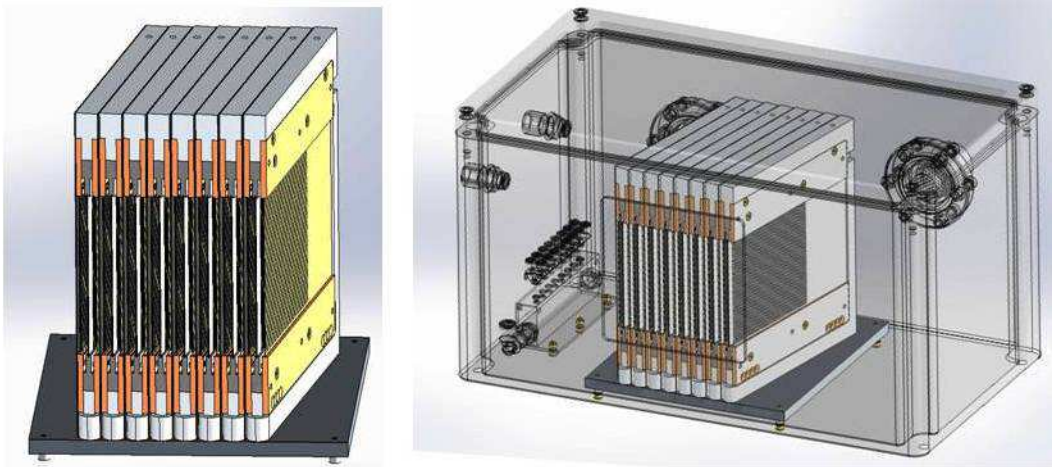


Figure 5. A 8-cassettes Multi-Blade in its gas vessel.

the wire plane edge a guard wire was installed to compensate the electric field distortion, hence this wire will not produce any signal.

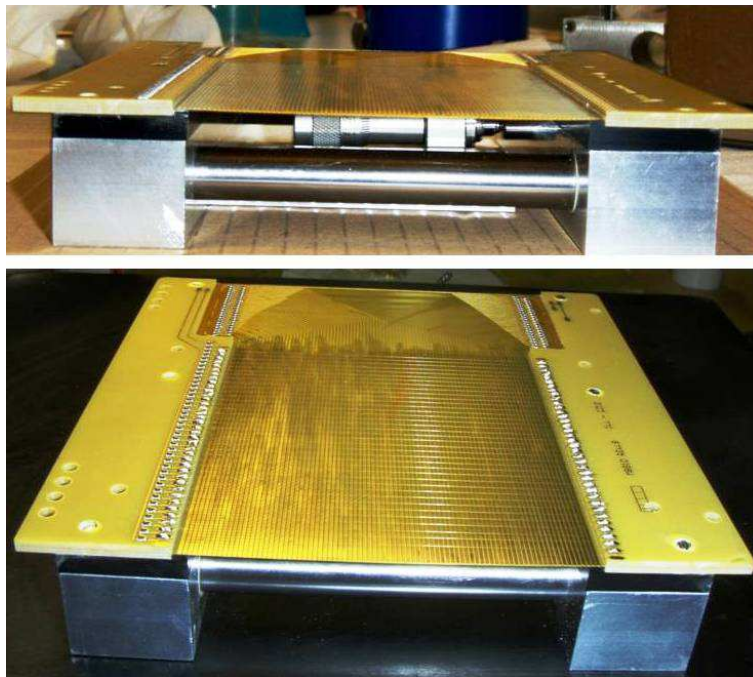


Figure 6. A polyimide PCBs where anode wires are mounted orthogonal to the cathode strips.

The total gap between the converter and the cathode plane, i.e. half cassette width, will be about 4 mm , thus any deformation of either the substrate or the strip plane will produce a variation in the local electric field produced between the anode plane and cathodes. Consequently where the cathode is closer to the wire plane the detector will manifest a higher gain. This effect mainly degrades the uniformity over the cassette surface. The overall uniformity on the whole detector surface is then degraded by the single cassette uniformity and their arrangement in the space: overlap and

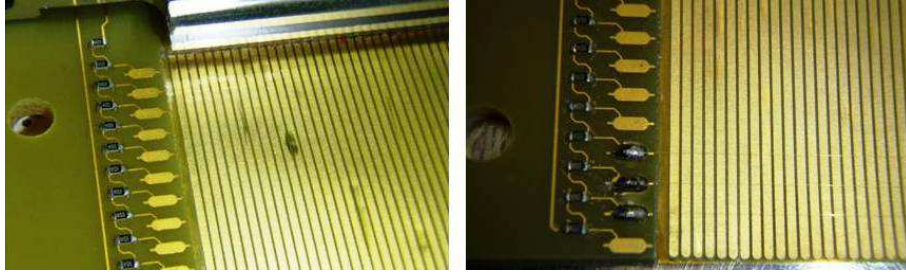


Figure 7. Detail of a polyimide PCBs: resistors for charge division link the wire pads where anodes are soldered.

switching from one to another.

It is crucial to control the flatness of both the substrate and the PCB. The first manufactured PCB was composed of a thin polyimide held on three sides by the rigid PCB. The provider was not able to assure the polyimide flatness with this design. We changed the PCB design in order to be able to pull on both sides and restore its flatness. The polyimide is held by only two of its sides (see Figure 6). The PCB is held by a tool (see Figure 6) that allows to stretch the foil before being mounted on the Aluminium holder. This tool allows also to mount wires on the PCB keeping the system under tension. The $15\ \mu\text{m}$ tungsten wires are mounted on the PCB under a tension of 35 g. Once wiring is over, the PCB can be installed on the holder.

Figure 8 shows the Aluminium holder where the double side coated substrate with $^{10}\text{B}_4\text{C}$ [14] is inserted. In order to keep the wire tension, the PCB, without removing the stretching tool, can be placed on the holder. The holder and the PCBs present four different fixation screw shifted by $0.25\ \text{mm}$ from each other. The PCB can be screwed on the holder according to its actual size after stretching. This ensures the right tension on the wires and the flatness of the cathode plane.

As for the read-out plane, the converter holding substrate must be flat too. After sputtering, between the Al -substrate and the $^{10}\text{B}_4\text{C}$ coating, a significant residual stress remains due to the difference in the thermal expansion coefficient of Al ($\sim 23.5 \cdot 10^{-6}\ 1/\text{K}$) and $^{10}\text{B}_4\text{C}$ ($\sim 5.6 \cdot 10^{-6}\ 1/\text{K}$). When they are cooled down to room temperature the Al contracts more than $^{10}\text{B}_4\text{C}$. Experiential evidences of that have been observed: on single side coated substrates, the un-coated side is shorter than the coated side, resulting into a bending of the blade. When a double-side coated blade has to be inserted into the holder (see Figure 8) the constraints on the sides make the blade bend and unstable. The gain in efficiency of using a double layer (option B) introduces some mechanical constraints which make its realization much more complicated than the implementation of the option A. We can deal with a reduced efficiency gaining in a mechanical simplicity.

We wanted to study both option A and B with this prototype but due to the blade mechanical issue we convert the prototype in a single layer detector.

In order to keep the substrate with the converter flat enough to ensure a uniform electric field, we mounted it on an Aluminium lid placed where a PCB was removed (see Figure 9). We used a $3\ \mu\text{m}$ thickness $^{10}\text{B}_4\text{C}$ coating instead. The gap between the wires and the converter was increased up to $6\ \text{mm}$, while the gap between the wires and the strips is about $2\ \text{mm}$. The MWPC is asymmetric. Figure 9 shows the four cassettes equipped with the read-out systems and the converters.

The version V1 of the Multi-Blade detector allowed only to study the single layer configuration A, as mechanical issues had made impossible the initial configuration B realization.



Figure 8. The Aluminium holder and a blade (substrate coated with $^{10}\text{B}_4\text{C}$ both sides) inserted.

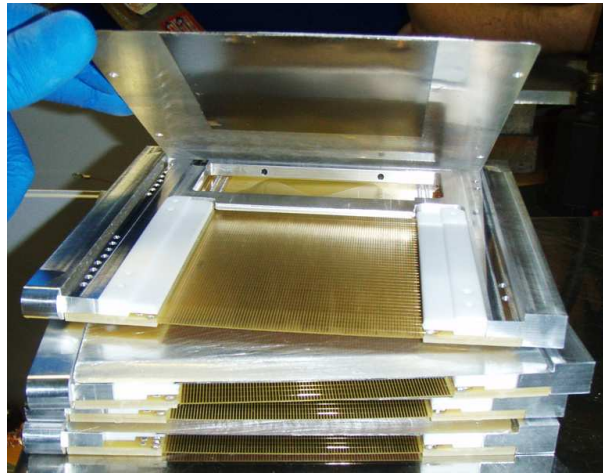


Figure 9. Four cassettes assembled. The read-out PCB is installed on the Aluminium holder.

The number of read-out channels per cassette were reduced from 8 to 4: 2 anode and 2 cathode outputs.

Four cassettes were stacked at 10° with respect to the beam and parallel to each other. Figure 10 shows the detail of the four cassettes stacked from two points of view. We define as the x -coordinate where the wire pitch is projected at 10° . The y -coordinate is defined by the direction orthogonal to the strips orientation.

The four cassettes were then installed in the gas vessel, see Figure 11. Each cassette is supplied by two inlets to let the gas flow directly inside them. The entrance window of the detector is the one on the right in Figure 11.

The front-end electronics of the prototype is connected outside the gas vessel and consists of a decoupling circuit and charge amplifiers. A schematic of the whole front-end electronic chain is shown in Figure 12. Both wires and strips are connected in the same way by their resistive chain, the AC signal is decoupled by two capacitors at both ends from the DC component used to polarize the wires at the HV and the strips to the ground potential.

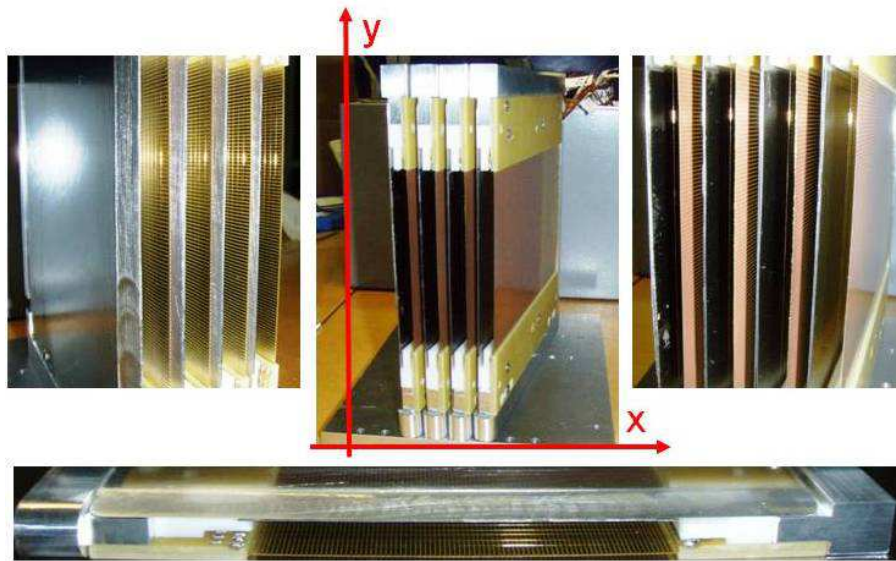


Figure 10. Four cassettes stacked one after the other at 10° and parallel each other.

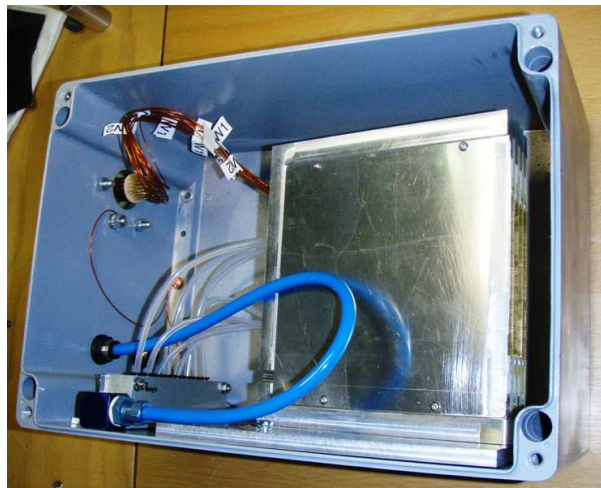


Figure 11. The four cassette assembly in the gas vessel. Each cassette is supplied by two gas inlets. The detector entrance window is the one on the right.

The charge is amplified by charge amplifiers. We used inverting amplifiers of $6V/pC$ and $1\mu s$ shaping time for anodes and non-inverting amplifiers of $32V/pC$ and $2\mu s$ shaping time for cathodes.

Each chain ends into two signal outputs that can be either summed to get the energy information (PHS) or subtracted and divided to get the positional information.

3.3 Results

3.3.1 Operational voltage

A counting curve was measured in order to set the right bias voltage to be applied to polarize the prototype. Each cassette output was connected to get the energy information and then to measure

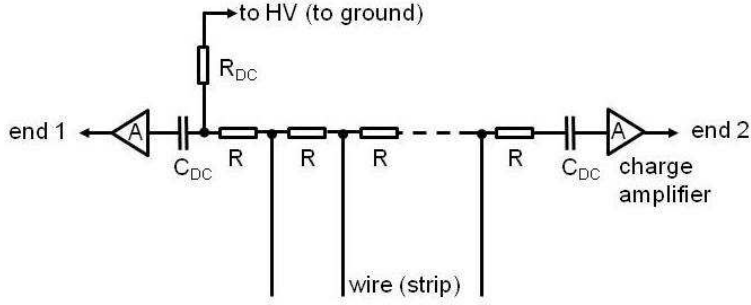


Figure 12. The Multi-Blade front-end electronics schematic.

the PHS. Given the electronic noise, a 25 mV threshold was used for the anode amplifiers; for the cathode amplifiers we used 100 mV . Figure 13 shows a PHS for both strips and wires, compared with a PHS calculated according to [13] at 1000 V .

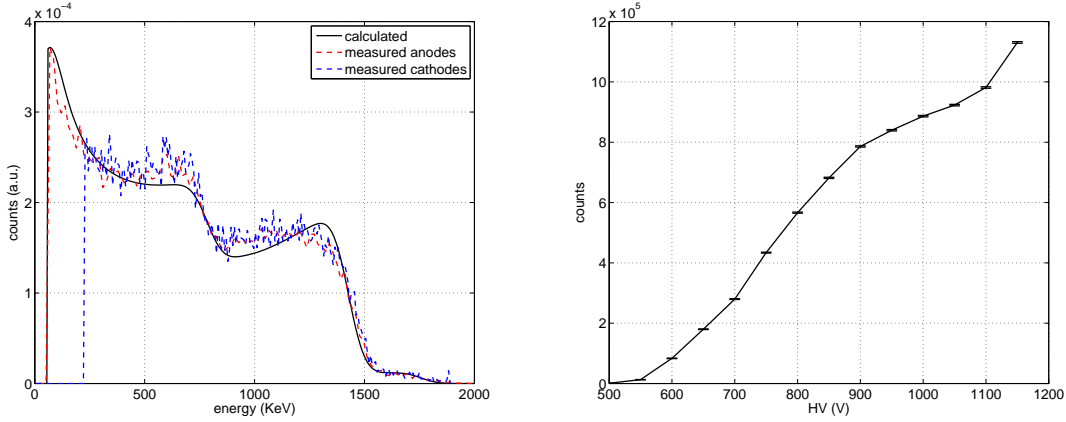


Figure 13. PHS measured on strips and wires at 1000 V and calculated PHS (left). The Multi-Blade detector plateau (right).

The working voltage chosen based on the counting curve is 1000 V .

3.3.2 Gain

The Multi-Blade prototype is operated in proportional mode, its gain has been measured on CT2 at ILL. The neutron flux of $(15280 \pm 20)\text{ neutrons/s}$ (2.5 \AA) was quantified using the procedure explained in details in [10].

The prototype was polarized at 1000 V . Its $3\text{ }\mu\text{m }^{10}\text{B}_4\text{C}$ converter layer was exposed to the beam orthogonally and $\Phi_d = (904 \pm 2)\text{ neutrons/s}$ were counted. It results into a $\varepsilon = (5.92 \pm 4)\%$ detection efficiency. The current flowing through the detector was measured and it is about $I_{prop.} = 180\text{ pA}$.

The detector operational voltage was set to 100 V . The measurement of the current output was repeated operating the detector in ionization mode, resulting into $I_{ion.} = 3.1\text{ pA}$.

The average charge created for a detected neutron both proportional and ionization modes are:

$$Q_{prop.} = \frac{I_{prop.}}{\Phi_d} = 199\text{ fC/neutron}, \quad Q_{ion.} = \frac{I_{ion.}}{\Phi_d} = 3.4\text{ fC/neutron} \quad (3.1)$$

This results into a gain of about $G = 58$ at $1000V$.

3.3.3 Efficiency

Detection efficiency of the Multi-Blade prototype V1 has been measured on CT2 at ILL by using a collimated and calibrated neutron beam of wavelength 2.5\AA .

The neutron beam was calibrated using an 3He -based detector as explained in [10]. After the calibration, the neutron flux the Multi-Blade was exposed to is (15280 ± 20) *neutrons/s* over an area of $2 \times 7\text{mm}^2$.

The efficiency was measured for the following bias voltages $950V$, $1000V$ and $1050V$. The efficiency was measured on the four cassettes under the angle of 10° and then averaged. The results are listed in Table 1.

Table 1. Multi-Blade detection efficiency at 2.5\AA for three bias voltages and calculated efficiency [13] for a given threshold.

| $HV(V)$ | $\varepsilon(\text{at } 2.5\text{\AA})$ | Threshold (KeV) | calculated $\varepsilon(\text{at } 2.5\text{\AA})$ |
|---------|---|---------------------|--|
| 950 | $(24.4 \pm 0.2)\%$ | 100 | 25.7% |
| 1000 | $(25.4 \pm 0.2)\%$ | 70 | 26.7% |
| 1050 | $(26.0 \pm 0.2)\%$ | 50 | 27.2% |

The result is in a good agreement with what can be calculated from the theory in [12] and [13] by using an energy threshold of $100KeV$, $70KeV$ and $50KeV$ for the three voltages from $950V$ to $1050V$ respectively. These thresholds have been determined from the comparison between the measured and calculated PHS [13], as shown in Figure 13 for the bias voltage of $1000V$.

3.3.4 Uniformity

The main issue in the Multi-Blade design is the uniformity over its active surface. The cassettes overlap to avoid dead zones, and, in the switching between one cassette to another, a loss in efficiency can occur. There are mainly two reasons that cause the efficiency drop: at the cassette edge the electric field is not uniform and there is some material that scatters neutron on the way to the next cassette. In order to reduce the dead zone at the cassette edge, i.e. any material that can cause scattering, each cassette is cropped (see Figure 10) to be parallel to the incoming neutron direction. Moreover, when a neutron is converted at the cassette edge, it produces a fragment that half of the time travels toward outside of the cassette and half time inward. We expect not to have generated charge for about 50% of the events. In addition to that the electric field at the edge may not be uniform and the guard wire contributes to enlarge the dead zone because it does not generate charge amplification.

We scan with a collimated neutron beam and we register a PHS over the whole prototype surface by using a 1mm step for the x -direction and a 10mm step for the y -direction. We integrate the PHS for each position and we obtain a local counting. We normalize it to 1 on the average efficiency. Figure 14 shows the relative efficiency scan over the whole detector. The scan along the cassettes in the position $y = 40\text{mm}$ is also shown.

Each cassette shows a quite uniform response along its strips (y -direction); the maximum efficiency

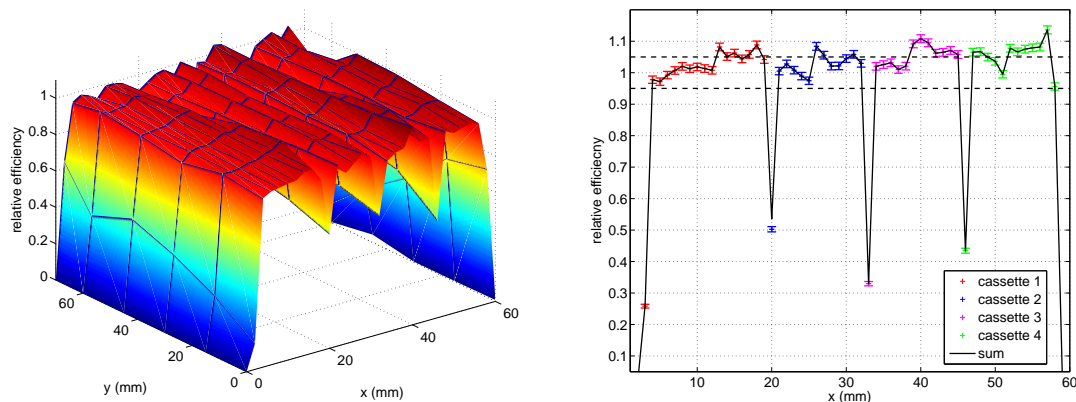


Figure 14. Relative efficiency scan over the whole detector surface.

relative variation is below 2%. On the other hand, in the gap between two cassettes the efficiency drops about 50% in a region which is 2 mm wide.

3.3.5 Spatial resolution

In order to calculate a detector spatial resolution one should be careful as to which definition has to be adopted in order to give a meaningful result. If the detector response is a continuous function or discrete the problem should be tackled in a different way.

Here we refer to [15] to properly calculate the spatial resolution given by the anodes (discrete response function) and to a standard Full Width Half Maximum (FWHM) definition for what concerns the cathodes (continuous response function) of the Multi-Blade prototype.

Spatial resolution: x The version V1 of the Multi-Blade prototype is operated at 10° between the neutron incoming direction and the detector converter layer. We recall that the wire plane is projected on the neutron incoming direction. An improvement by a factor $\sin(10^\circ) \sim 0.17$ is achieved on the horizontal spatial resolution with respect to an orthogonal incidence. E.g. if the spatial resolution, before projection, were a wire pitch (in our prototype 2.5 mm) this results in an actual resolution of about 0.45 mm.

In Figure 15 the charge division response of the wire plane is shown by using either a diffuse beam or a collimated beam down to 1 mm footprint (2.5\AA).

The charge division method is able to identify each wire anode position; when a collimated beam is in one position we can either get a single wire or two wires reacting. This effect is due to the fact that the wire plane splits the gas volume into almost independent cells, thus the charge generated by primary ionization in one cell makes its associated wire react. In our case, since we are using a mixture of Ar/CO_2 (90/10) at atmospheric pressure the ^{10}B neutron capture reaction fragment ranges make a few mm. Therefore, if the track is contained in one single wire cell, only a single wire reacts; on the other hand if the track travels across two cells we get a two wire response. Since the wire plane is read-out in charge division, if two wires react, the hit will be identified to be in between the two wires, corresponding to the charge centroid. The response distribution, for a given beam position, will have tails corresponding to these events. Figure 15 shows the resulting

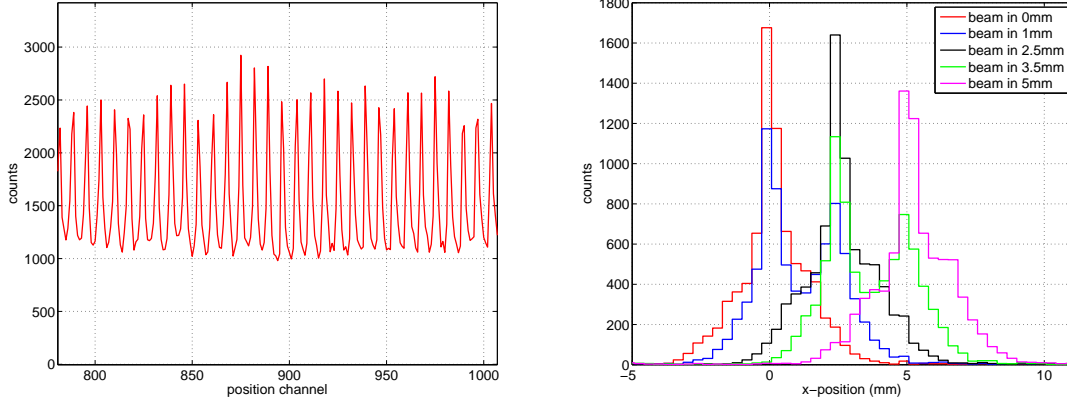


Figure 15. Diffuse beam wire response in charge division (left), collimated neutron beam response as a function of the beam position (right).

distribution as the neutron beam moves along the detector. One can wonder now what is the actual spatial resolution in this situation. In order to quantify it is necessary to apply the informational-theoretical approach of [15].

We calculate the mutual information between the distribution in Figure 15 for all the possible combinations and we will take as resolution the worse result at an information threshold level of 0.47 bits which corresponds to the FWHM criterion of a continuous distribution.

Figure 16 shows the mutual information as a function of the distance of the neutron distribution response of our detector for different reference positions [15]. We notice that in the worst case we end up with 3.4mm ; which translates into a spatial resolution of 0.6mm at 10° .

Note that the spatial resolution lies in between a single wire pitch (2.5mm) and two.

Spatial resolution: y As already mentioned, particle tracks in our gas make a few mm . Since the cathodes read-out strips are 0.8mm wide and they are spaced by 0.2mm and the read-out is performed by a charge division chain, there are several strips that are involved in the induction process per event. The charge division determines the charge centroid along the y -direction in the detector.

For the cathodes the response can be considered continuous and the FWHM method is suitable.

Figure 17 shows the strip response as a function of the position of the collimated beam hitting the detector. By performing a gaussian fit we obtain a spatial resolution (FWHM) for the vertical direction y of about 4.4mm .

4. Multi-Blade version V2

4.1 Mechanical study

We learned from the Multi-Blade version V1 that the single layer configuration (option A) presents less mechanical constraints. Moreover, the substrate holding the converter has not to be crossed by neutrons that makes its manufacture easier.

The converter layer can be thick because the efficiency is saturated above $3\ \mu\text{m}$; the substrate can be

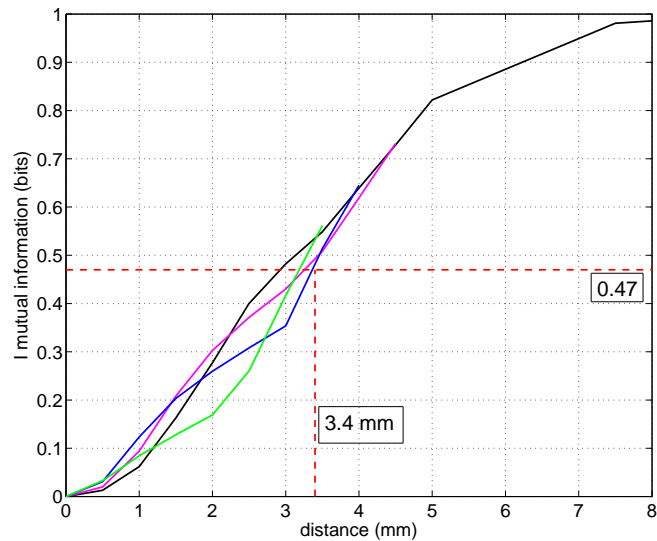


Figure 16. Mutual information as a function of the distance between the response distributions of the neutron detector. The horizontal line defines an information of 0.47 bits that corresponds to a 3.4 mm spatial resolution (before projection) in the worse case.

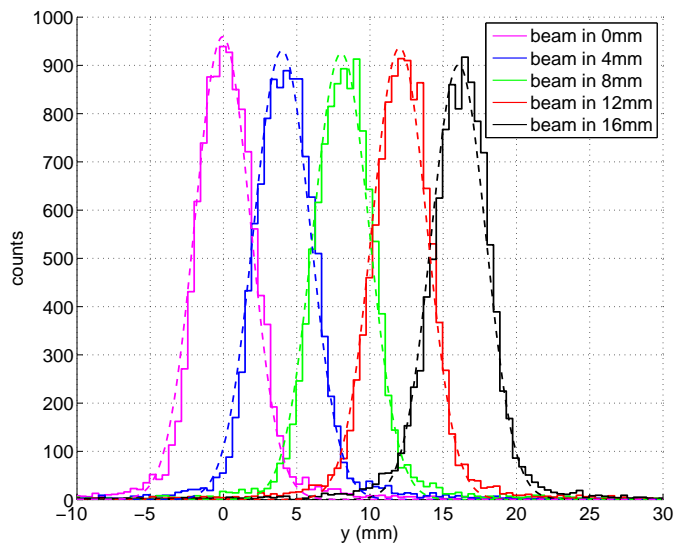


Figure 17. Fine beam neutron scan along the strip cathodes. The spatial resolution is given by the FWHM and corresponds to 4.4 mm.

thick also because it has not to be crossed by neutrons to hit a second converter. Hence, the substrate can be an integrated part of the cassette holder, the converter layer can be directly deposited over its surface. The read-out system used is the same as in version V1. Neutrons have still to cross the PCBs before being converted. Figure 18 shows a cassette and a stack of them conceived for the single layer option.

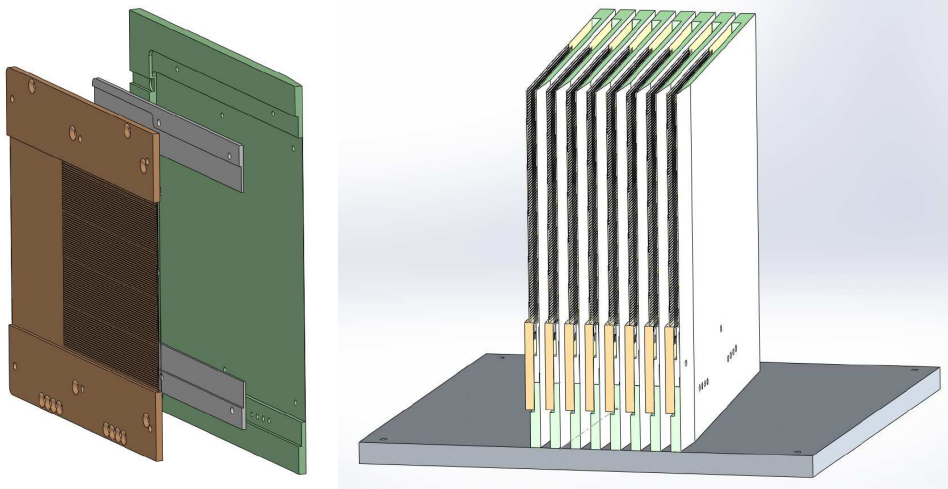


Figure 18. A cassette conceived to hold one converter layer (left) and a stack of several cassette (right).

The cassettes are oriented at 5° with respect to the incoming neutron direction. The sensitive area of each cassette is $10 \times 9 \text{ cm}^2$ but, the actual sensitive area offered to the sample is given by $(10 \text{ cm} \cdot \sin(5^\circ)) \times 9 \text{ cm} = 0.9 \times 9 \text{ cm}^2$. As a result, the actual projected wire pitch is improved down to 0.22 mm .

4.2 Mechanics

The second prototype (V2) consists also of four cassettes but we operate them at 5° . At this inclination the expected efficiency at 2.5 \AA is about 43% if we employ the sputtered coating of the version V1 [14]. The cassettes are the ones shown in Figure 18, conceived to study the single converter layer option. A rigid substrate is directly coated with the converter material. The cassette width in the version V1 was about 12 mm , in the version V2 we reduce their actual size to 6 mm . Consequently the MWPC gap, between the converter and the cathodes, is 4 mm . With respect to the version V1 the wire plane is closer to the converter.

The prototype active area, considering the cassette overlap, is about $3.2 \times 9 \text{ cm}^2$.

The read-out PCBs are those used in the version V1.

Figure 19 shows a cassette substrate both coated and un-coated.

Since the efficiency is saturated as the thickness of the layer exceeds $3 \mu\text{m}$, we study the possibility to use different converters. We can deposit a painting containing ^{10}B grains and make a coating a few hundreds of microns thick. A thick layer also functions as an integrated collimator. Any neutron that comes from the sides of the detector has less probability to be detected and is more likely absorbed in the outer layers. Hence, only neutrons which impinge the detector from the front have a serious chance to generate a signal. Neutron background is then decreased.

The uniformity of the coating, even in the single layer configuration, is an important aspect to guarantee the converter flatness. The latter has to ensure the precision of the neutron incidence angle, in fact if it varies slightly the efficiency changes widely. Furthermore, a deviation from the converter flatness also induces the variation of the electric field and then the local gain of the detector changes.



Figure 19. A cassette V2 coated and un-coated with ^{10}B painting.

The roughness of the converter should be below the neutron capture fragment ranges, which is of the order of a few μm for ^{10}B . In fact, the gain in efficiency due to an inclination comes from the fact that the neutron path travels close under the surface. If the surface is irregular (on the μm scale or more), that can be seen as equivalent for a neutron to hit a surface perpendicularly, there is not much gain in efficiency. It is crucial that the size of our grains, in the painting, is less than the particles ranges, i.e. their size should be below the micron scale for ^{10}B .

The conductivity of the painting can be an issue. If the resistivity is too large the charge evacuation is not guaranteed and consequently the actual electric field is affected. We mix a glue with ^{10}B grains of sizes $\sim 10\mu\text{m}$. We did not have access to a finer-grained ^{10}B powder: our grinding technique resulted in $\sim 10\mu\text{m}$ grain size. We used this powder. As the grain size is not smaller than the fragment ranges we know that there can be an efficiency issue. The layer resistivity was measured to be about $50\text{M}\Omega \cdot \text{m}$ and for a 0.5mm thick layer.

Figure 20 shows two PHS: one is taken with a $3\mu\text{m}$ thick $^{10}\text{B}_4\text{C}$ layer [14] and the other with the ^{10}B painting both installed in a MWPC, at normal incidence and with a 2.5\AA neutron beam. The difference in gain on the two spectra is due to the difference in the gas gap between the wire plane and the converter, since the painting is a few mm closer to the wires than the sputtered layer.

The painting efficiency is 1.5% lower than the sputtered coating.

In order to investigate if the resistivity of the painting is not too large to avoid the evacuation of the charges, we place the painting layer on a very intense beam of 560KHz and we measure the counting rate as a function of time. There are no losses after several hours. The resistivity of the ^{10}B painting seems to be acceptable.

The painting is suitable for single layer application supposed that we can control the flatness of the layer and to use smaller grains. We do not guarantee the sputtered layers efficiency for our prototype under an angle because of the size of the grains we used in the painting.

The converter painting was not optimized, hence we expect some problems due to its not perfect regularity. This effect will be more evident at the edge of each cassette where the flatness affect to a greater extent the electric field glitches.

We mount the prototype using the painting. Four cassettes were assembled. Figure 21 and 22 show the cassettes and the installation in the gas vessel for testing.

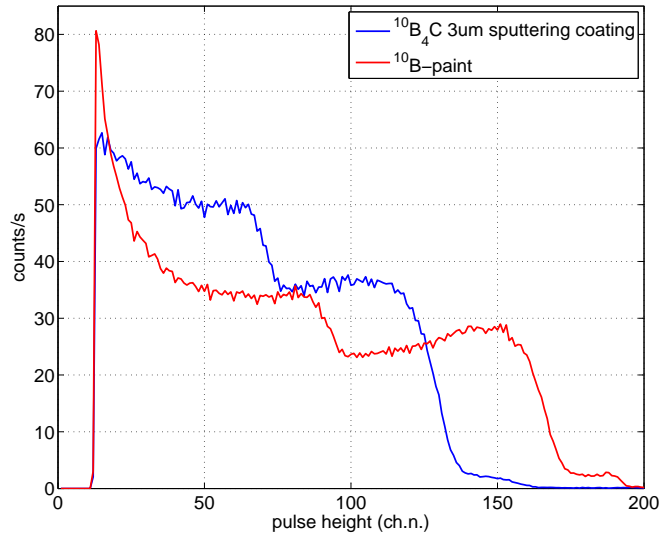


Figure 20. Comparison between the PHS of the sputtered coated layers [14] and the ^{10}B painting.

The electronics used is the same as in the version V1 of the Multi-Blade.

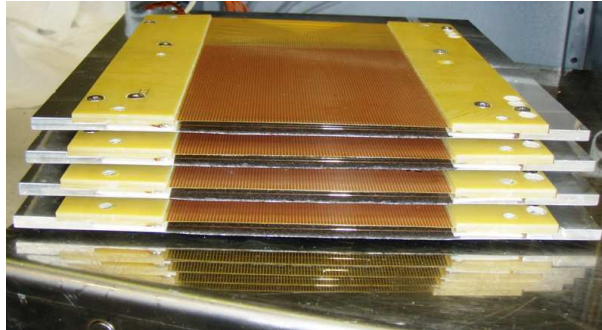


Figure 21. Four fully assembled cassettes for the Multi-Blade version V2.

4.3 Results

4.3.1 Operational voltage

The measure of the counting curve gives the bias voltage of 800V .

The operational voltage is lower than the one used for the first prototype because the gap between anodes and cathodes was reduced in the new design. For this reason the PHS is degraded also because the maximum path in Ar/CO_2 of an α -particle makes almost 9mm it is more likely in the version V2 to hit the opposite cathode before depositing its entire energy in the gas volume.

4.3.2 Efficiency

Detection efficiency of the Multi-Blade prototype V2 has been measured on CT2 at ILL by using a collimated and calibrated neutron beam of wavelength 2.5\AA using the procedure explained in [10].

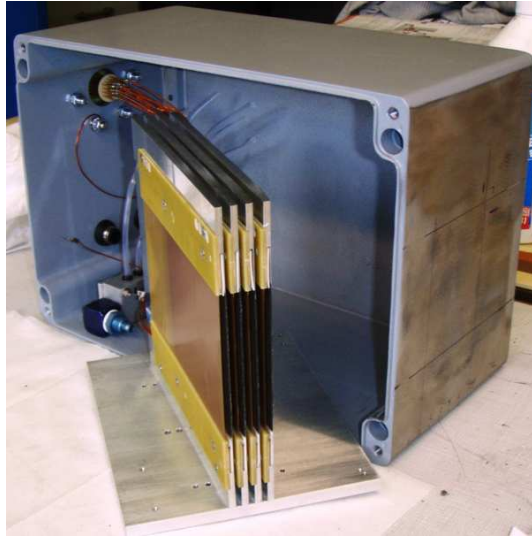


Figure 22. The four cassettes installed at 5° with respect to the detector window being installed in the gas vessel.

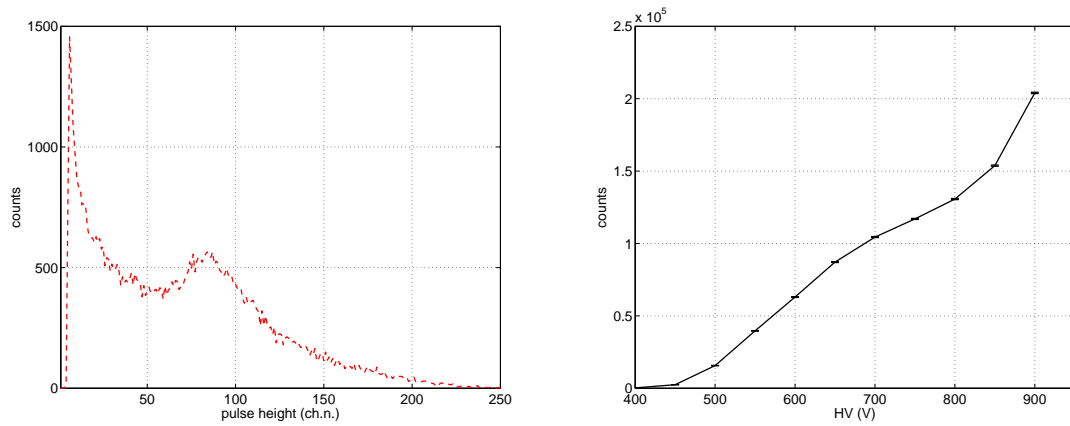


Figure 23. PHS measured on wires at 800V (left). The Multi-Blade detector plateau (right).

The neutron flux used is (12010 ± 20) neutrons/s over an area of $2 \times 6 \text{ mm}^2$.

The efficiency was measured for the operational voltage 800V. The efficiency was measured on the four cassettes under the angle of 5° and then averaged. The results is:

$$\varepsilon (\text{at } 2.5\text{\AA}) = (8.32 \pm 0.05) \% \quad (4.1)$$

The expected efficiency for a sputtered layer of which the roughness is widely below the μm scale is about 43% (at 2.5\AA). In our case, however the inclination only increases the efficiency by a few percent because of the grains size. The surface irregularity makes the inclination effect vanish. Neutrons only impinge almost perpendicularly on the microscopic grain structure.

By using a sputtered layer [14] or, if one can better control the painting flatness and have smaller grain size, there should be no reason not to get the calculated efficiency.

4.3.3 Uniformity

In the version V2 of the Multi-Blade the mechanics is more compact in order to avoid dead zones in the overlap between the cassettes. It has been discussed that the two issues which degrade the uniformity are those dead zones and the electric field at each cassette edge.

Even though the mechanics design is more efficient in the version V2, the electric field issue remains.

Moreover, the coating done by the painting was slightly irregular mostly at the edges of each cassette. This diminishes the precision by which we switch between one and the following. A large amount of converter material at the edge will absorb most of the neutrons without generating any signal.

Figure 24 shows the relative efficiency scan over the detector surface. Compared with the version V1 uniformity is worse. The gap between the converter and the wire plane is 2mm , hence any irregularity on the layer surface will affect the local gain of the detector. Even along each cassette (y-direction) the gain varies by about 10% while in the sputtered version it only varied of about 2%.

Moreover, now looking at the x-direction, at the cassettes edge the efficiency now drops more than 50%. This is due to the amount of converter at the edge that does not generate signal but only absorbs neutrons.

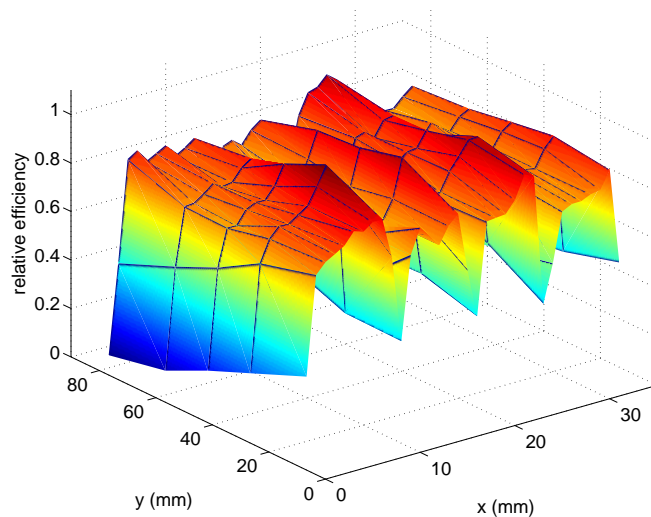


Figure 24. Relative efficiency scan over the whole detector surface.

The version V2 is in principle more compact and if the coating would be precise the uniformity was expected to be better than in the version V1.

4.3.4 Spatial resolution

The spatial resolution was calculated as already shown for the Multi-Blade version V1 according to [15]. By using a very collimated beam, of about $0.2 \times 10\text{mm}^2$, we scan one cassette and a half

of the detector. Each step is 0.9mm along the x -direction. The cassette 1 is from $x = 0\text{mm}$ to $x = 10\text{mm}$, the cassette 2 starts at $x = 10\text{mm}$. Figure 25 shows the reconstructed image and its projection on the x -direction obtained by adding together all the images taken in the scan.

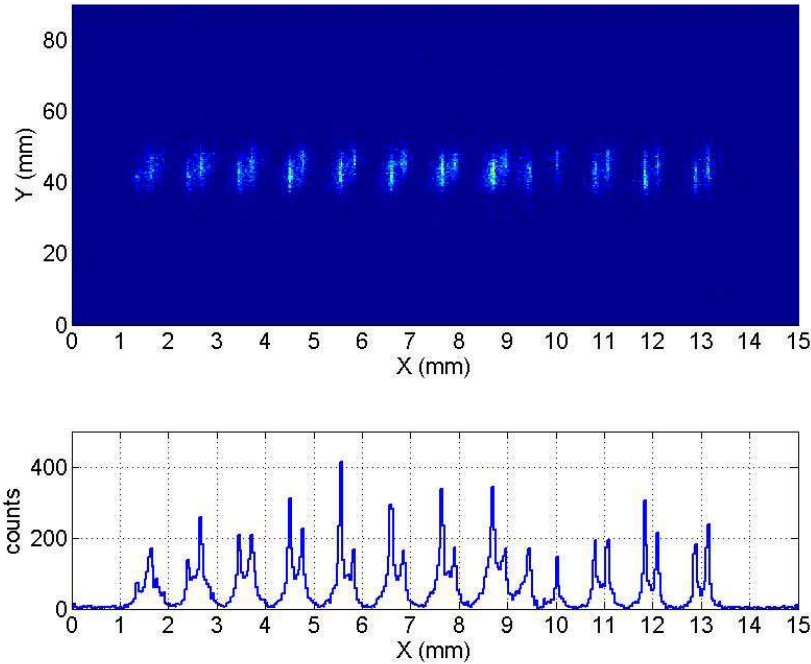


Figure 25. An image and its projection on the x axis taken with the prototype. Each slit is $0.2\text{mm} \times 10\text{mm}$ large and it is spaced by 0.9mm .

For each step either a wire or two are firing. At the switching point between the two cassette we observe the drops in the counts.

Spatial resolution: x We quantify the spatial resolution along the x -direction in the same way as for the version V1.

We scan the detector surface to obtain the events distribution to calculate the mutual information [15] which is shown in Figure 26. We use the threshold of 0.47bits which corresponds to the standard FWHM resolution definition and we obtain a value of 3.16mm .

This value is slightly better of the one found for the version V1 because in the version V2 the gap between wires and converter is diminished. It is the first part of the ionization path, on average, that gives more signal and it is closer to the fragment emission point, this improves the spatial resolution.

Since the detector is inclined at 5° the actual spatial resolution is given by the projection: $3.16\text{mm} \cdot \sin(5^\circ) = 0.275\text{mm}$.

Spatial resolution: y The spatial resolution given by the strips is also enhanced thanks to the narrower gas gap.

Figure 27 shows a scan performed along y . The spatial resolution is given by the FWHM and is 4mm .

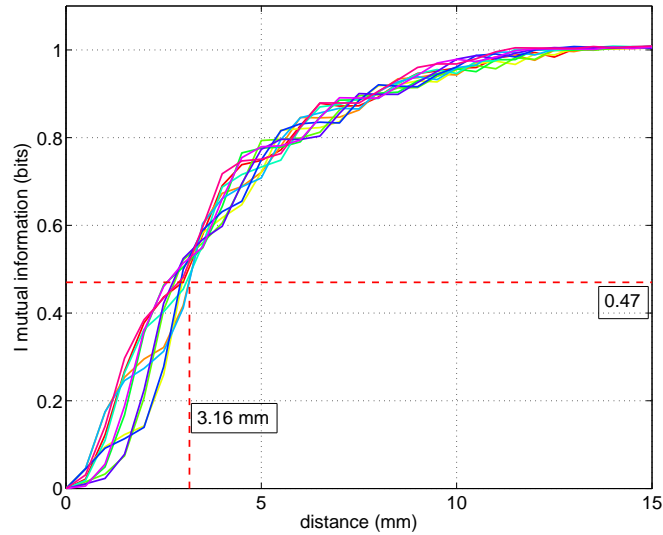


Figure 26. Mutual information as a function of the distance between the response distributions of the neutron detector. The horizontal line defines an information of 0.47 bits that corresponds to a 3.16 mm spatial resolution (before projection) in the worse case.

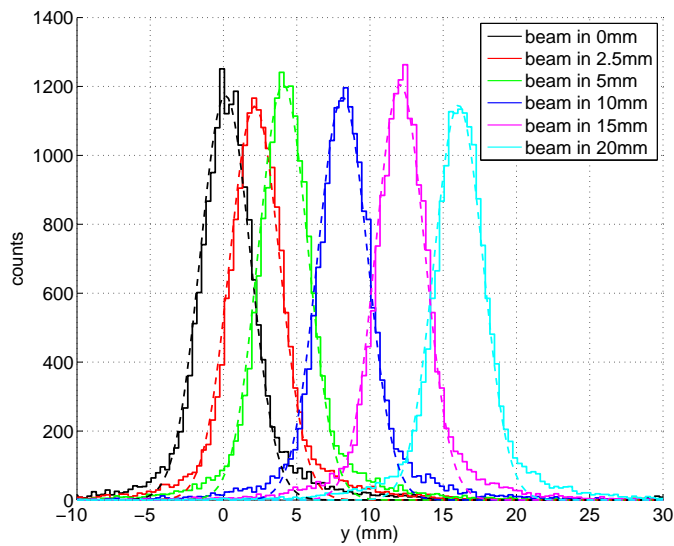


Figure 27. Fine beam neutron scan along y . The spatial resolution is given by the FWHM and corresponds to 4 mm.

4.3.5 Dead time

The intrinsic dead time of a detector is due to its physical characteristics; here we measure the entire dead time from the detector to the end of the whole electronic chain.

Neutrons arrive at the detector according to an exponential distribution assuming the process to be Poissonian. A way to measure dead time is to record the difference in the arrival time between two

successive neutrons on the detector; in principle their distribution should follow an exponential:

$$f(t) = \frac{1}{\tau} e^{-t/\tau} \quad (4.2)$$

where the time τ represents the average time is in between two events; $\nu = 1/\tau$ is the counting rate. In practice the detector is characterized by a dead time t_D which is the minimum time interval that separates two correctly recorded events. As a result the distribution measured with the detector should move away from the theoretical behavior near and below t_D . Moreover, if the detector is ideally non-paralyzable, the distribution has to show a sharp cutoff at t_D because the probability of measuring an event between $t = 0$ and $t = t_D$ is zero.

In a paralyzable case the passage is smoother.

Figure 28 shows the measured times between neutrons on the detector. The two anode outputs of a single cassette were added and the resulting signal discriminated. The time between every couple of discriminated events was recorded for $T = 300$ s.

The measurement was performed by using two kind of amplifiers. One is the standard Multi-Blade amplifier of $1 \mu\text{s}$ shaping time and the second is a fast amplifier with 3 ns shaping time.

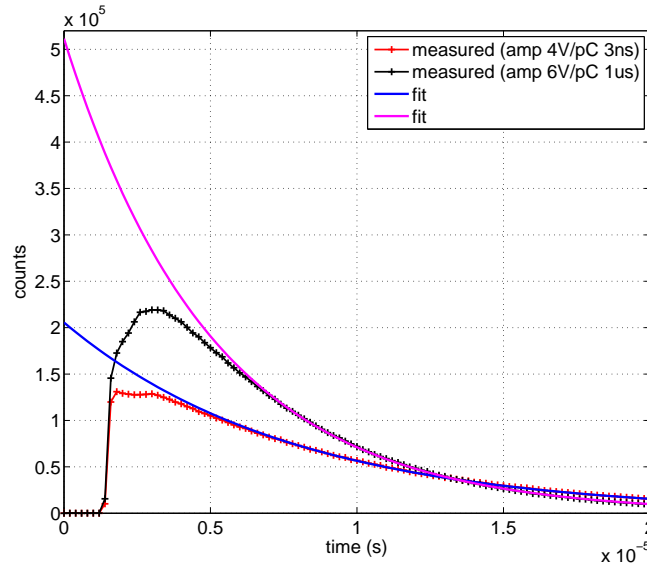


Figure 28. Time distribution of neutron events recorded with the Multi-Blade, the fit shows the theoretical behavior. Two anode amplifiers have been used.

The fits in Figure 28 represent the theoretical behavior.

The value for τ , for both the measured distributions, was obtained by the calculation of the maximum likelihood estimator for the exponential distribution. It is:

$$\tau = \frac{\sum_i n_i (t_i - t_s)}{\sum_j n_j} \quad (4.3)$$

where t_s is the minimum time for which we consider the measured distribution to behave as expected. We can assume that a time t_s exists above which the measured distribution follows the

exponential behavior. We assume $t_s = 7 \mu s$.

By knowing τ and the measurement duration $T = 300 s$, the total number of neutrons that have generated a signal in the detector but, due to dead time, have not all been recorded, is given by $N_0 = \frac{T}{\tau}$. If we integrate instead the measured distribution we obtain the number of events recorded N_m . The dead time is simply given by:

$$t_D = \frac{N_0 - N_m}{N_0} \tau = \frac{\frac{T}{\tau} - N_m}{T} \tau^2 \quad (4.4)$$

For the $1 \mu s$ amplifier we obtain $t_D = (1.58 \pm 0.08) \cdot 10^{-6} s$, the fast amplifier gives $t_D = (1.5 \pm 0.1) \cdot 10^{-6} s$.

5. Conclusions

The Multi-Blade detector is a promising alternative to 3He -based detectors, to accomplish the high spatial resolution and the high count rate capability needed in the new applications of neutron reflectometry. Two prototypes have been developed and assembled at ILL to show we can overcome the reasonable limits of 3He -based detectors in terms of spatial resolution.

Exploiting solid ${}^{10}B_4C$ -layers operated in a proportional gas chamber, it can attain a suitable detection efficiency for neutron reflectometry applications. A single ${}^{10}B_4C$ conversion layer is operated at grazing angle with respect to the incoming neutron direction. This configuration has at least three advantages: the detection efficiency is increased, the neutron flux is split between many wires and, the most important, the spatial resolution improved.

In order to get a suitable detection efficiency, compared to 3He , the converter layers must be operated at an angle of 10° or below.

We studied two approaches to be used in the Multi-Blade implementation: either with one or with two converters. The latter has more technical issues that makes its realization more difficult. The single layer detector is finally the choice to make to keep the mechanics reasonably simple. The extra advantage of having only one converter is that the coating can be of any thickness above $3 \mu m$ without affecting the efficiency, while for the two layer option its thickness should be chosen carefully. Moreover, in the two layer configuration the substrate choice is also crucial because it should be kept as thin as possible to avoid neutron scattering and this leads to mechanical issues. In a single-layer detector it can be integrated in the holding structure. Moreover, since the efficiency is saturated as the thickness of the single-layer exceeds $3 \mu m$, we can make a coating a few hundreds of μm thick. A thick layer also functions as an integrated collimator. Any neutron that comes from the sides of the detector has less probability to be detected with respect to those impinging the detector from the front. Neutron background is then decreased.

We conceived a detector to be modular in order to be versatile: it is composed of modules called *cassettes*. We operated the two Multi-Blade prototypes at either $\theta = 10^\circ$ and $\theta = 5^\circ$. In each of the solutions proposed for the cassette concept the read-out system has to be crossed by neutrons before reaching the converter. The mechanical challenge in the read-out system construction is to minimize the amount of material on the neutron path to avoid scattering that can cause misaddressed events in the detector. The choice fell on polyimide substrates. It can be eventually replaced with more suitable materials.

The detector is operated at atmospheric pressure. This makes it suitable to be operated in vacuum. Moreover, cost effective materials can be used inside the detector because outgassing is not an issue.

Since the detector is modular the main issue is its uniformity. In the presented prototype we got about 50% drop in efficiency in the overlap region between cassettes.

The presented Multi-Blade showed a very high spatial resolution, it was measured to be about 0.3 mm in one direction and about 4 mm in the other one.

We measured the neutron detection efficiency for both prototypes at 2.5 Å neutron wavelength. The first prototype has an efficiency of about 28% employing sputtered $^{10}\text{B}_4\text{C}$ -layers inclined at 10° . This result is in a perfect agreement with the expected efficiency [12], [13]. Since the efficiency, in the single layer option does not depend on the converter thickness above $3\ \mu\text{m}$, in the second prototype we investigated a different deposition method: a ^{10}B glue-based painting. This thick painted layer functions also as an integrated collimator inside the detector. The resistivity of the ^{10}B painting is larger than the sputtered $^{10}\text{B}_4\text{C}$ -layers but it seems to be acceptable and does not cause issues to the charge evacuation. We measured the efficiency of the second prototype operated at 5° and we only got about 8%. The coarse granularity of the painting makes the inclination effect vanish. The expected efficiency for a sputtered layer of which the roughness is widely below the μm scale is about 43% (at 2.5 Å). There is no reason not to get the calculated efficiency with a suitable painting.

We measured the detector dead time, including the read-out electronics, to be about 1.5 μs .

The single layer option represents a good candidate to push the performances of ^3He detectors. Further studies need to address the uniformity problems. If a simple coating technique is found, e.g. painting containing grains of a suitable size that assures a uniform layer, the Multi-Blade could be a cost-effective and high performance alternative. Its production is easy to be implemented.

Acknowledgments

The author (F.P.) would like to thank the entire neutron detector group (SDN) at ILL for the practical and intellectual support given to develop the work contained in this article. In particular a special thank goes to B. Guérard, the detector group head at ILL, who first had the idea of the Multi-Blade detector [8] who gave the possibility to the author to work on this subject. Specifically we would like to thank J.C. Buffet and Q. La Manna for the mechanical designs, S. Cuccaro for the mechanical support, J.F. Clergeau and J.M. Rigal for the help in developing the electronics.

The authors want also to thank the Thin Film Physics Division of Linköping University (Sweden) - especially C. Höglund, - for the Boron Carbide coatings.

References

- [1] S. Peggs, *ESS Technical Design Report*, ESS-doc-274, 23 April 2013. ISBN 978-91-980173-2-8, <http://eval.ess.lu.se/cgi-bin/public/DocDB/ShowDocument?docid=274>.
- [2] B. Gebauer et al., *Towards detectors for next generation spallation neutron sources*, Proceedings of the 10th International Vienna Conference on Instrumentation, Nuclear Instruments and Methods in Physics Research Section A: Accelerators, Spectrometers, Detectors and Associated Equipment, Volume 535, Issues 1-2, 2004, Pages 65-78, 0168-9002, 10.1016/j.nima.2004.07.266.

- [3] R. A. Campbell et al., *FIGARO: The new horizontal neutron reflectometer at the ILL*, The European Physical Journal Plus, Springer-Verlag, Volume 126, Issue 11, 2011, Pages 1-22, 10.1140/epjp/i2011-11107-8.
- [4] R. Cubitt et al., *D17: the new reflectometer at the ILL*, Journal of Applied Physics A, Springer-Verlag, Volume 74, Issues 1, 1 December 2002, Pages s329-s331, 10.1007/s003390201611.
- [5] J. Stahn et al., *Focusing specular neutron reflectometry for small samples*. Eur. Phys. J. Appl. Phys., Volume 58, 2012, 10.1051/epjap/2012110295.
- [6] R. Cubitt et al., *Neutron reflectometry by refractive encoding*, The European Physical Journal Plus, Springer-Verlag, Volume 126, Issues 11, 11 November 2011, Pages 1-5, 10.1140/epjp/i2011-11111-0.
- [7] R. Cubitt et al., *Refraction as a means of encoding wavelength for neutron reflectometry*. Nuclear Instruments and Methods in Physics Research Section A: Accelerators, Spectrometers, Detectors and Associated Equipment, Volume 558, 2006, Pages 547-550, 10.1016/j.nima.2005.12.045.
- [8] J.C. Buffet et al., *Advances in detectors for single crystal neutron diffraction*, Nuclear Instruments and Methods in Physics Research Section A: Accelerators, Spectrometers, Detectors and Associated Equipment, Volume 554, Issues 1-3, 1 December 2005, Pages 392-405, ISSN 0168-9002, 10.1016/j.nima.2005.08.018.
- [9] J.C. Buffet et al., *Study of a 10B-based Multi-Blade detector for Neutron Scattering Science*, Nuclear Science Symposium and Medical Imaging Conference (NSS/MIC), Transaction Nuclear Science Conference Record IEEE - Anaheim, 2012, PAGES 171-175, ISSN 1082-3654, 10.1109/NSSMIC.2012.6551086.
- [10] J. Birch et al., *$^{10}\text{B}_4\text{C}$ Multi-Grid as an Alternative to ^3He for large area neutron detectors*, IEEE T. Nucl. Sci., Volume PP, Issue 99, 17 January 2013, Pages 1-8, ISSN 0018-9499, 10.1109/TNS.2012.2227798.
- [11] M. Henske et al., *The 10B based Jalousie neutron detector – An alternative for ^3He filled position sensitive counter tubes*, Nucl. Instrum. Meth. A, Volume 686, 11 September 2012, Pages 151-155, ISSN 0168-9002, 10.1016/j.nima.2012.05.075.
- [12] D. S. McGregor et al., *Design considerations for thin film coated semiconductor thermal neutron detectors—I: basics regarding alpha particle emitting neutron reactive films*, Nuclear Instruments and Methods in Physics Research Section A: Accelerators, Spectrometers, Detectors and Associated Equipment, Volume 500, Issues 1-3, 11 March 2003, Pages 272-308, ISSN 0168-9002, 10.1016/S0168-9002(02)02078-8.
- [13] F. Piscitelli et al., *Analytical modeling of thin film neutron converters and its application to thermal neutron gas detectors*, Journal of Instrumentation, Volume 8, P04020, April 2013, 10.1088/1748-0221/8/04/P04020.
- [14] C. Höglund et al., *B_4C thin films for neutron detection*, J. Appl. Phys., Volume 111, Issue 10, 23 May 2012, Pages 10490-8, ISSN 0168-9002, 10.1063/1.4718573.
- [15] P. Van Esch et al., *An information-theoretical approach to image resolution applied to neutron imaging detectors based upon discriminator signals*, Proceeding of ANNIMA, 2013, arXiv:1307.7507.